Evaluation of rosette infrasonic noise-reducing spatial filters

Michael A. H. Hedlin[a)]
Institute of Geophysics and Planetary Physics, Scripps Institution of Oceanography, University of California, San Diego, La Jolla, California 92093-0225

Benoit Alcoverro
Commissariat a l'Energie Atomique, Departement Analyse et Surveillance de l'Environnement, BP 12, 91680 Bruyeres le Chatel, France

Gerald D'Spain
Marine Physical Laboratory, Scripps Institution of Oceanography, University of California, San Diego, La Jolla, California 92093-0225

(Received 13 June 2002; revised 10 June 2003; accepted 12 June 2003)

This paper presents results from recent tests of rosette infrasonic noise-reducing spatial filters at the Pinon Flat Observatory in southern California. Data from 18- and 70-m aperture rosette filters and a reference port are used to gauge the reduction in atmospheric wind-generated noise levels provided by the filters and to examine the effect of these spatial filters on spatially coherent acoustic signals in the 0.02- to 10-Hz band. At wind speeds up to 5.5 m/s, the 18-m rosette filter reduces wind noise levels above 0.2 Hz by 15 to 20 dB. Under the same conditions, the 70-m rosette filter provides noise reduction of up to 15 to 20 dB between 0.02 and 0.7 Hz. Standing wave resonance inside the 70-m filter degrades the reception of acoustic signals above 0.7 Hz. The fundamental mode of the resonance, 15 dB above background, is centered at 2.65-Hz and the first odd harmonic is observed at 7.95 Hz in data from the large filter. Analytical simulations accurately reproduce the noise reduction and resonance observed in the 70-m filter at all wind speeds above 1.25 m/s. Resonance theory indicates that internal reflections that give rise to the resonance observed in the passband are occurring at the summing manifolds, and not at the inlets. Rosette filters are designed for acoustic arrivals with infinite phase velocity. The plane-wave response of the 70-m rosette filter has a strong dependence on frequency above 3.5 Hz at grazing angles of less than 15° from the horizontal. At grazing angles, complete cancellation of the signal occurs at 5 Hz. Theoretical predictions of the phase and amplitude response of 18- and 70-m rosette filters, that take into account internal resonance and time delays between the inlets, compare favorably with observations derived from a cross-spectral analysis of signals from the explosion of a large bolide. [DOI: 10.1121/1.1603763]

PACS numbers: 43.28.Dm, 43.28.Ra, 43.50.Cb [LCS]

I. INTRODUCTION

A. Infrasound and the new global monitoring system

A natural consequence of any global nuclear-test ban treaty is the need for global monitoring for clandestine nuclear testing activity. In the case of the recent Comprehensive Nuclear-Test-Ban Treaty, which bans nuclear explosions of any yield, four monitoring networks will be used—seismic, hydroacoustic, air acoustic (or infrasound), and radionuclide as part of an International Monitoring System (IMS). This study relates to the infrasound component of the IMS. Each of the 60 arrays planned for the infrasound network will comprise up to 8 sensors.

Because of wind-generated turbulence, the atmosphere is inherently noisy at frequencies of interest to the nuclear monitoring community (between 0.01 and 10 Hz). As a result, it is necessary to suppress infrasonic wind noise at each station in the infrasound network. IMS infrasound stations are currently being equipped with spatial noise-reducing systems (Daniels, 1959; Burridge, 1971; Grover, 1971; Alcoverro, 1998) similar to those depicted in Fig. 1. The infrasound network is to provide enough sensitivity to allow discrimination of nuclear tests from myriad other atmospheric events worldwide. Reduction of atmospheric noise is therefore of paramount interest to the monitoring community.

B. Infrasonic signals

The physics of propagation of sound through the atmosphere defines, to a large degree, the noise-reduction problem. Since the era of atmospheric testing of nuclear weapons, it has been known that the shock front from a nuclear explosion will evolve into infrasonic energy that propagates efficiently through the lower atmosphere (Landau and Lifshitz, 1959). Buried nuclear tests cause a piston-like vertical ground motion that also produces infrasonic pressure waves (Blanc, 1985; Calais *et al.*, 1998). Much of the acoustic energy from an infrasound source in the lower atmosphere (0–50-km altitude) is refracted back to the Earth's surface in the stratosphere (between ~20- to 50-km altitude) or at lower altitudes due to wind shear (Simons, 1995). A Lamb surface wave exists principally below ~30-km altitude (Lamb, 1932;

a)Electronic mail: hedlin@ucsd.edu

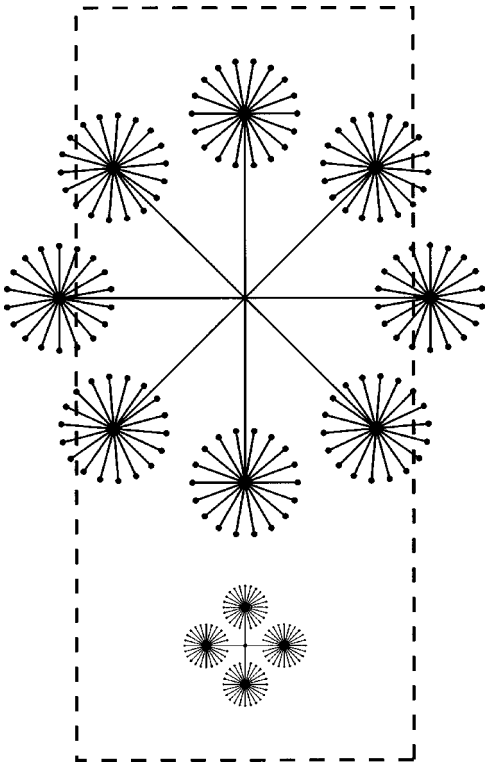

FIG. 1. Two rosette filters considered in this paper are shown to scale with a National Football League playing surface. The 18-m filter comprises 92 low-impedance inlets in 4 rosettes. The 70-m filter comprises 144 inlets arranged in 8 rosettes. In both filter designs, the inlets are connected by solid pipe to secondary summing manifolds at the center of each rosette. The secondary manifolds are connected to a primary manifold which is connected by a short pipe to the sensor. Each inlet is located the same distance along solid pipe from the sensor. Signals arriving from directly above the filter are summed in phase. Adjacent ports in the 70-m filter are separated by 2.79 m. Adjacent ports in the 18-m filter are 0.85 m apart.

Francis, 1973) and can be observed globally (Blanc, 1985). Most signals propagate across Earth's surface with phase velocities below 360 m/s (McKisic, 1997). These phase velocities are consistent with an arrival direction within 15° of the horizontal; i.e., near-grazing arrival angles are most common, particularly for long-range sources. The frequency content of infrasonic energy is strongly range dependent due to atmospheric absorption (Blanc, 1985). Most signals of interest to the monitoring community lie between 0.01 and 10.0 Hz (Zumberge *et al.*, 2003). At these frequencies, signals from remote sources are highly coherent at spacings of tens to hundreds of meters. Noise that results from atmospheric turbulence near the recording site is incoherent at spacings of tens of meters (Priestley, 1966).

C. Noise suppression

Although it is generally accepted that the study of acoustic signals in the atmosphere requires suppression of noise due to atmospheric turbulence, how this is best accomplished is a matter of vigorous debate. Spectral filtering is generally ineffective as turbulent noise spans the entire frequency band of interest to the monitoring community (Kaimal and Finnigan, 1994). It has been recognized since the 1950's that the disparate correlation lengths of most signals and noise can be exploited to improve the ratio of signal to noise. The prototypical spatial filter, proposed by Daniels (1959), consists of a single 603-m-long tapered pipe. The pipe was tapered to eliminate internal acoustic reflections back to the sensor. Acoustic energy entered the Daniels pipe via N high-impedance inlets distributed uniformly along its length. Assuming spatially incoherent noise, and perfectly spatially coherent signal, the amplitude ratio of coherent signal to incoherent noise is predicted to improve by $N^{1/2}$. The filter with 100 inlets was found to reduce atmospheric noise at the theoretical limit of 20 dB at wind speeds up to 13 m/s (Daniels, 1959), suggesting perfectly uncorrelated noise between the inlets. Although proven to be effective at improving the reception of signals, the Daniels line microphone is inherently directional if the wavelength of the signal is less than the sensor length (i.e., near 1 Hz or above).

With the possibility of clandestine nuclear testing at any azimuth from a recording station, subsequent designs use several relatively short pipes distributed in azimuth (Davidson and Whitaker, 1992). Alcoverro (1998) proposed a filter which consists of several clusters, or rosettes, of low-impedance inlets. Each inlet in a cluster is connected to a ''secondary'' summing manifold by a solid pipe. A solid pipe connects each secondary summing manifold to one primary summing manifold or directly to the sensor (Fig. 1).

D. Rationale for the present study

As development of the IMS global infrasound network surges ahead, there is a pressing need for intercomparisons of filter designs currently in use at IMS arrays, and between existing and new designs that have been proposed for use at future array sites. It is necessary to assess the utility of these filters for reducing noise due to atmospheric turbulence while preserving the coherent signals of interest to the nuclear monitoring and scientific communities. In this paper, we present our findings regarding the utility of 18- and 70-m rosette filters at attenuating noise while preserving signal. The large, 70-m, rosette filters have been built at IMS infrasound array sites near Warramunga, Australia and at Pinon Flat, California. Empirical observations of noise reduction are compared with theoretical predictions. We point out some limitations of the rosette filter design and suggest possible avenues for improving the performance of these filters.

II. THE PINON INFRASOUND TEST BED

All of our experiments have been conducted at the infrasound test bed at the Pinon Flat Observatory in southern California (Figs. 2 and 3). The observatory is located in the Anza Borrego desert in California's coastal ranges 125 km to the northeast of San Diego and 50 km to the southwest of Palm Springs. The observatory is useful for studies of infrasonic noise-reducing systems as there are strong diurnal and seasonal changes in meteorological conditions at this site. Wind speeds are often near zero at night and sometimes exceed 15 m/s during the day. Winds are most commonly from the northeast or the southwest. The desert is sparsely vegetated with Pinon pine trees and there is essentially no low-lying ground cover. The observatory is accessible at all times of the year. The International Monitoring System (IMS) in-

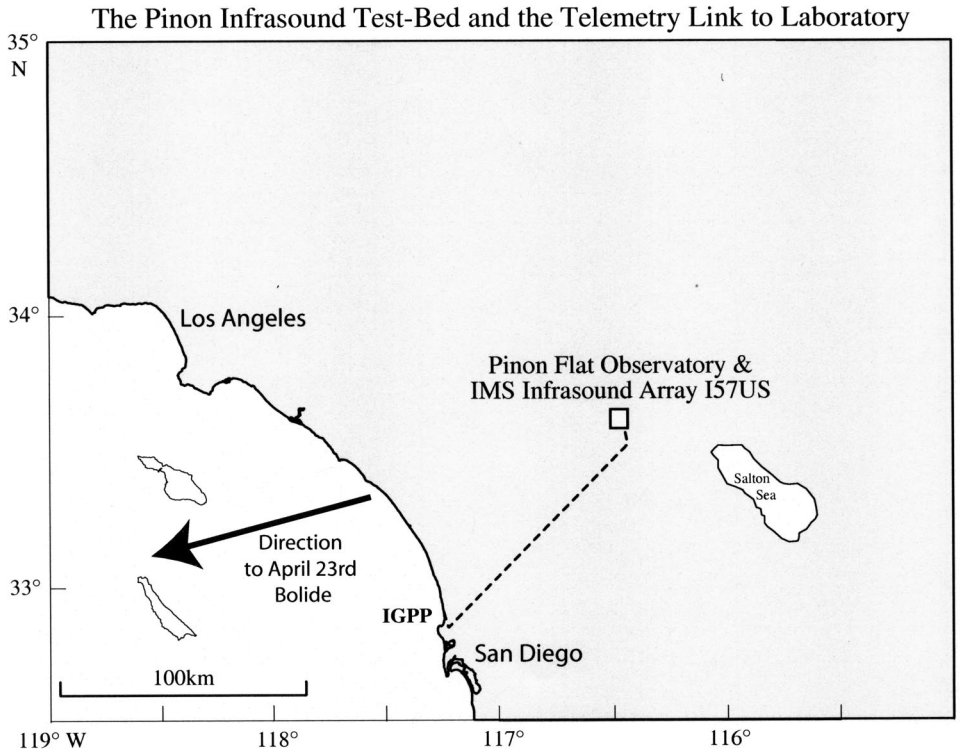

FIG. 2. The IMS infrasound array, 157US, is located in the Anza Borrego desert at the Cecil H. and Ida M. Green Pinon Flat Observatory (PFO). The infrasound test bed is located at PFO. The real-time radio-telemetry link to the laboratory (IGPP) is also shown. Signals from a large bolide that exploded to the SW of the observatory are used in this paper to calibrate the rosette filters.

frasound array I57US is located at PFO (Fig. 3). The 2-km aperture array comprises eight instruments and includes both 18-m noise-reduction rosette filters (designed to detect signals between 0.2 and 5 Hz) and 70-m-aperture filters (sensitive to low-frequency signals between 0.02 and 3 Hz). An IMS auxiliary three-component seismic station is located at the northwest corner of the observatory. There is essentially no cultural noise in the area.

III. EXPERIMENTAL LAYOUT

A typical experimental layout is pictured in Fig. 4. At each site we use the MB2000 aneroid microbarometer fabricated by the French Departement Analyze et Surveillance de l'Environnement (DASE) and now by Tekelec. These sensors provide an electrically filtered signal between 0.01 and 27 Hz (low-passed below 9 Hz by our antialiasing filter) with an adjustable sensitivity. The version used in our experiments had a sensitivity of 20 mV/Pa. The electronic noise of the sensor is 2 mPa rms, between 0.02 and 4 Hz, which is well below measured noise levels at PFO. Each sensor was placed in an insulating case and was attached to one of three systems. In total, this experiment used five sensors. Three sensors were each attached to a single low-impedance inlet located 5 cm above the ground and provided the spatially unfiltered reference data. One sensor was located near the auxiliary seismic station (Fig. 3). The two other reference sites were colocated with the 18-m rosette filter at site H1 and the 70-m rosette filter at L2 (Fig. 3). The two other sensors were attached to the rosette filters at H1 and L2. The ''reference'' sensor near the seismic station, and the sensors at H1 and L2 were colocated with an ultrasonic anemometer for wind velocity, air temperature, and humidity sensors. The temperature and humidity sensors were located 1 m above the ground. The wind sensor was 2 m above the ground at all sites. In this experiment, the infrasound and meteorological signals were digitized at 20 and 1 sps, respectively, using a 24-bit Reftek 72A-08 data acquisition system. Each system was powered by solar energy or by buried power lines. Data from three sites were transmitted in real time via a 2.2-GHz spread-spectrum radio link to our laboratory in La Jolla (Fig. 2). Data from two of the sites were transmitted along telephone lines. The experiments were preceded by calibration tests in the field at PFO, and in the laboratory at the Institute of Geophysics and Planetary Physics in La Jolla, California. The tests were conducted to ensure all field systems were robust and yielded equal digitized signals for equal input.

IV. OBSERVATIONS OF INFRASONIC NOISE REDUCTION

The first goal of this paper is to compare the capability of the different rosette filters at reducing infrasonic noise levels. To make this comparison, the filtered pressure records at each site are divided into 15-m intervals (e.g., Fig. 5). A Welch time-averaged pressure spectrum (Welch, 1967) is calculated from each 15-min segment of data. The Welch estimator reduces the variance of the power spectral estimate relative to a periodogram by averaging several spectral estimates taken from overlapping segments of data. The test of the rosette filters spanned more than 768 h and thus yielded 3074 15-min nonoverlapping segments of data. The pressure spectral estimates are binned by wind speed and stacked to reduce the statistical uncertainty inherent in the spectral estimation process. The stacked spectra clearly reveal the dependence of average noise levels on wind speed. Although wind-speed data are collected at all sites, for the purpose of comparing data collected at the same time at the different

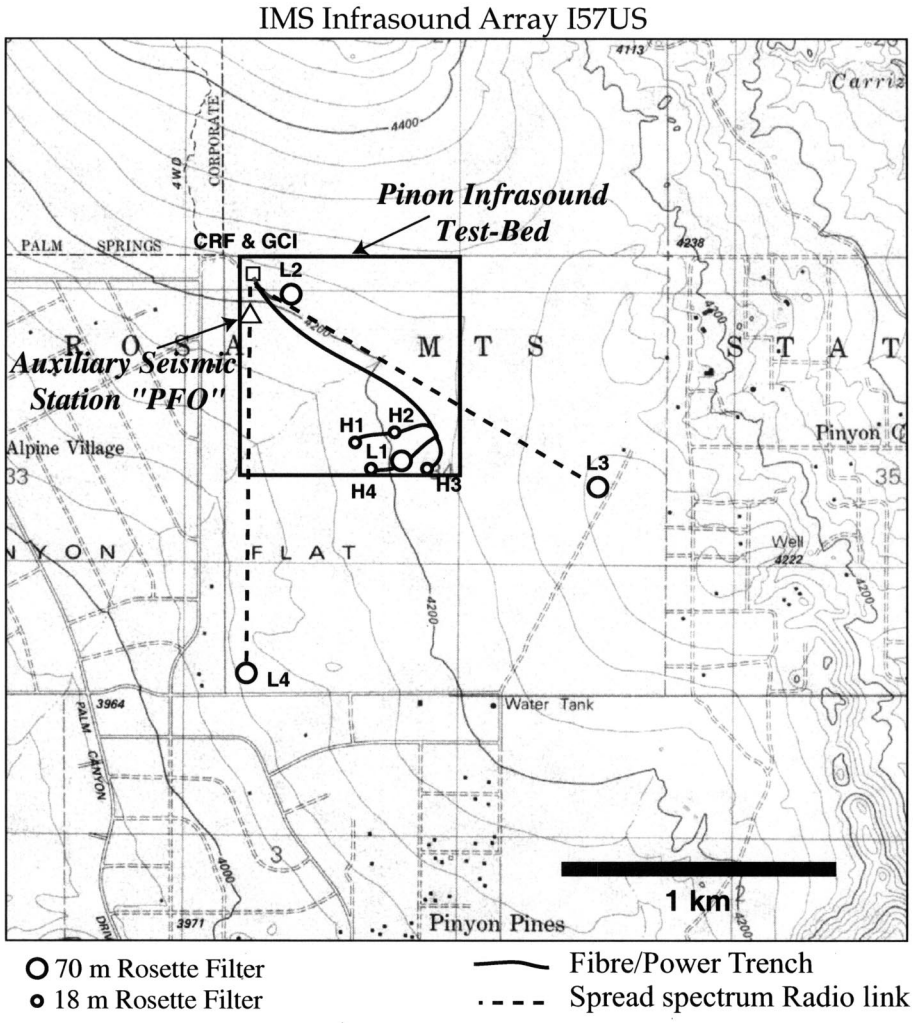

FIG. 3. The eight-element infrasound array at Pinon Flat, California comprises four long-period elements (L1 through L4) in a centered triangle spanning less than 2 km and four short-period elements (H1 through H4) in an irregular quadrilateral near the center. The terrain slopes down gently to the southwest. The contour interval is 40′.

sites, only the wind-speed data collected at 2 m at the reference port is used in the binning process. The wind speeds at the 18-m filter were reduced somewhat by the forest (Fig. 6). The 15-min average wind speeds plotted in this figure show clearly the diurnal variations in the wind speed at all sites. The experiment began during adverse weather conditions. Data were lost near day 10 due to a fault in the telemetry system.

The spectral estimates are binned into 0.5-m/s wind-speed intervals starting at 0.0 m/s (Figs. 7 and 8). The lowest curve in each panel in Fig. 7 corresponds to estimates taken when the wind at the reference site was less than 0.5 m/s. At the three sites, we see infrasonic noise increases at all frequencies with increasing wind speed. The microbarom peak (the spectral peak near 0.2 Hz) is most clearly resolved by the 70-m rosette filter. The peak is seen clearly at wind speeds up to 1.5 to 2.0 m/s and in some individual spectra at wind speeds up to 2.5 m/s. The effectiveness of this filter at reducing infrasonic noise below 1 Hz is evident in Fig. 8. Direct comparison of the stacked spectra taken from the reference port near the seismic station and 70-m rosette data streams indicates reduction of noise by 15 to 20 dB at frequencies below 1.0 Hz. The 18-m rosette filter averages noise over a smaller area and is less effective at low frequencies. The noise-reduction performance of the 18-m filter, however, surpasses the 70-m filter at frequencies above 0.5 Hz.

The stacked spectra in Fig. 7 indicate that the 18-m rosette filter is ineffective at average wind speeds (3.0 to 3.5 m/s) at frequencies below 0.1 Hz. Above 0.5 Hz, the noise reduction is near the theoretical limit for uncorrelated noise of 19.8 dB ($10 \log 10[1/N]$, where N is 96). At wind speeds above 2 m/s, and at frequencies above 1 Hz, the apparent noise reduction of the 18-m filter exceeds this limit. The reference inlet for this experiment was not colocated with the 18-m filter but was located in an area with no vegetation. The 18-m filter was surrounded by Pinon pine trees. As a result, high-frequency noise levels at the reference site are slightly higher, giving the appearance of greater noise reduction than actually occurred. The binned spectra reveal a clear increase in the frequency at which the 18-m filter reduces noise levels with increasing wind speed. At 1.0 to 1.5 m/s, noise reduction is observed at 0.05 Hz. By 5.0 to 5.5 m/s, noise reduction is not observed until 0.2 Hz.

Chi-squared statistics were calculated for the stacked spectra but are not shown here. The bins contain enough stacked spectra that the uncertainty in the spectral levels is insignificant relative to the observed differences in the noise levels between the noise-reduction systems.

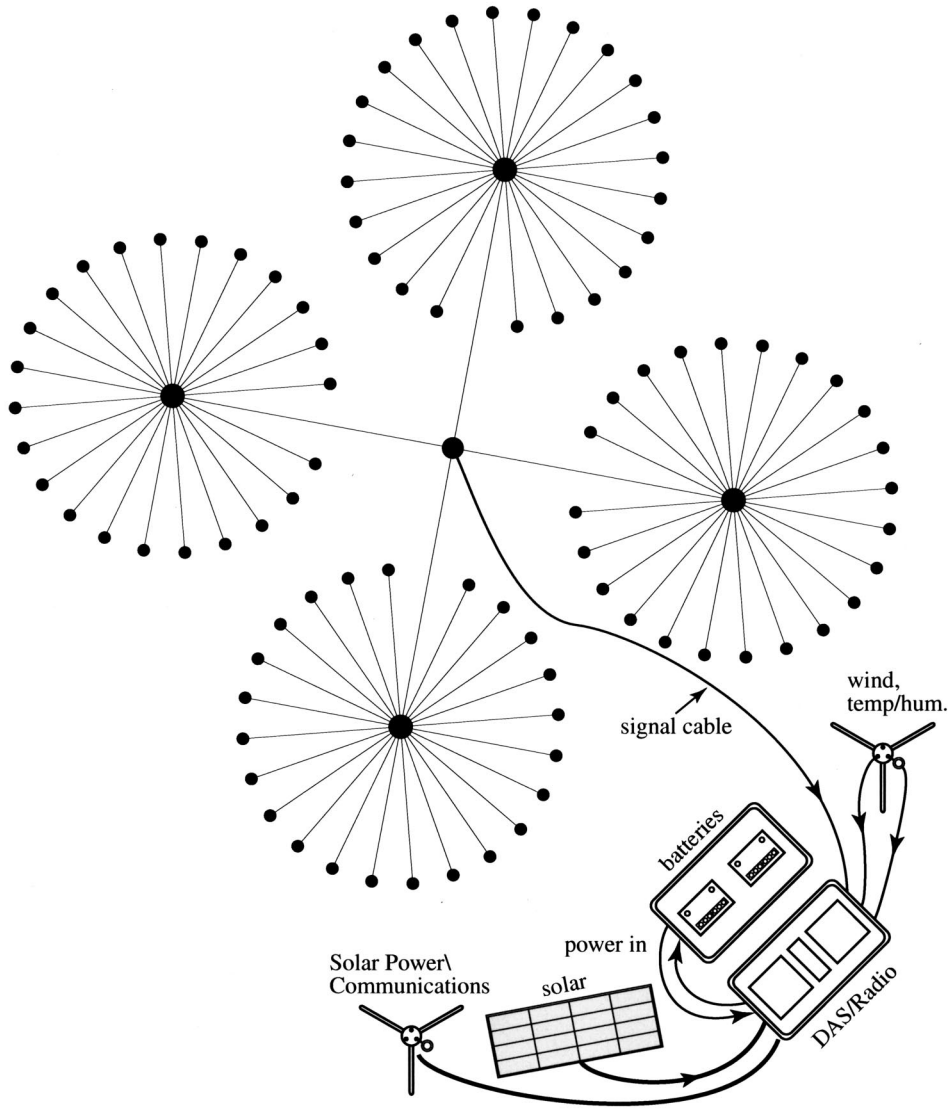

FIG. 4. A typical experimental recording site consists of a filter and a sensor. In this example, the sensor is represented by the black dot at the center of the filter. The digitizer and spread-spectrum radio are located in one enclosure, batteries are in a second. Wind speed and direction are sensed at 2-m elevation; humidity and temperature data are collected at 1-m elevation on the same mast. Data are transmitted in real-time via a 2.2-GHz spread-spectrum link back to the laboratory in La Jolla (Fig. 2). Solar energy powers all systems.

V. RESONANCE IN ROSETTE FILTERS

A. Observations of resonance

The stacked spectra reveal the effectiveness of the filters at reducing low-frequency infrasonic noise. The spectra also plainly show evidence of resonance within the rosette filters. Resonance in the 18-m filter is relatively minor and is only evident above 3.0 Hz near the Nyquist frequency. The resonance peaks in data from the 70-m filter are significant, however, and lie well within the frequency band of interest to the nuclear monitoring community. Resonance peaks are observed at 2.65 and 7.95 Hz. The second resonance peak is observed at 3.00 times the frequency of the first peak. The resonance peaks are nearly independent of wind speed (Fig. 9) and temperature. From 0 to 35 °C, the frequency of the first peak rises 1.5%, the second rises 0.8%. The very weak dependence on air temperature is expected as the pipes are buried and are therefore not exposed to the larger changes in air temperature recorded by the temperature sensor.

Resonance in the 70-m filter is seen at all wind speeds. As shown in Fig. 10, at a time when wind speeds were <0.25 m/s, the constant high-frequency resonance obscures the infrasonic pressure variations recorded via a nonresonant spatial filter. This nonresonant microporous hose filter spanning an area 70-m across is described more fully in Herrin *et al.* (2001).

B. Modeling resonance peaks in the 70-m filter

Reflections will occur inside the rosette pipe system at points where the acoustic impedance changes. These points are located at the inlets, all summing manifolds, and at the sensor. In the 70-m rosette filter tested in this experiment, the segment between the sensor and the primary summing manifold is 2.85 m long. At 27 °C the speed of sound in free space is 347 m/s. The speed of sound in narrow conduits 8–10 mm in radius at frequencies between 0.1 and 10 Hz is difficult to estimate as in this frequency band neither the large-tube or small-tube approximations of Benade (1968) are considered to be highly accurate. The dimensionless parameter r_v (which gives the ratio of the conduit radius and the viscous boundary layer thickness) ranges from 1.9 (at 0.1 Hz) to 19 (at 10 Hz). The two approximations place the propagation speed of sound at frequencies from 1 to 10 Hz between 288

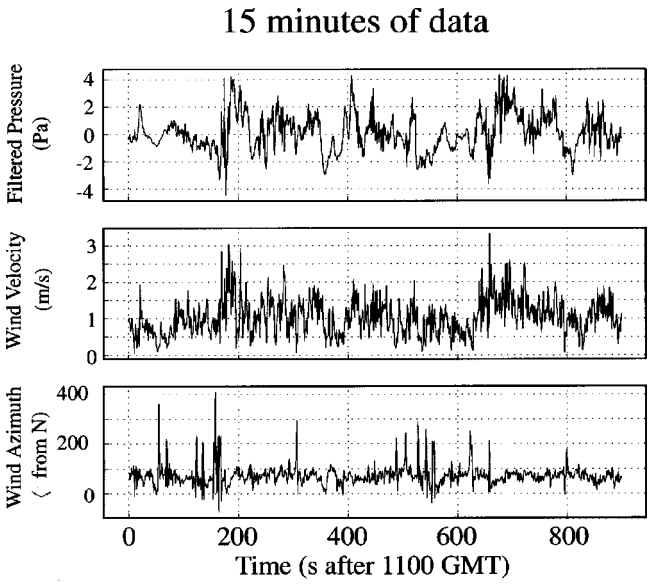

FIG. 5. Atmospheric pressure and wind data from a 15-min interval starting at 11:00 GMT at the reference site. The pressure data are filtered between 0.01 and 9.0 Hz and are sampled at 20 sps. The meteorological data are collected once per second.

and 324 m/s. The average of the two estimates is 306 m/s. Assuming this velocity for the propagation of sound waves in the pipe, the natural frequency of resonance along this segment lies far beyond the Nyquist frequency and could not produce the spectral peaks in the data. The resonance that gives rise to the spectral peaks observed in Fig. 8 occurs in the rosettes between the inlets and the secondary summing manifolds or between the primary and secondary manifolds. The rosette filter resonates at the fundamental and the first odd harmonic (at 2.65 and 7.95 Hz, respectively). Presumably, higher overtones would be observed if the data were sampled more rapidly than 20 sps. The resonance in the 70-m rosette filter is akin to organ-pipe resonance. Assuming two-way length of 54 m (double the distance between the primary and secondary summing manifolds), and a propagation velocity of 306 m/s, we would expect the fundamental mode at 2.83 Hz and the first odd overtone centered at 8.49 Hz. The closeness of these estimates to the observed values strongly suggests that the resonance that gives rise to the observed spectral peaks occurs between the primary and secondary summing manifolds. We can rule out resonance within the rosettes as the cause of the observed spectral modulations as the fundamental resonance frequency for resonance between the secondary manifolds and the inlets is predicted to lie at 9.5 Hz.

More exact modeling of the response of the 18- and 70-m rosette filters across the entire frequency band of interest to the monitoring community requires consideration of the boundary conditions at the reflection points, attenuation of propagation of sound through all elements of the rosette pipe system, and a statistical characterization of the noise field across the area spanned by the filter. This has been done by Alcoverro (1998) and will be considered in the next section.

VI. WIND-NOISE REDUCTION SIMULATIONS

As described in Alcoverro (1998), the use of nonporous hoses in the rosette noise-reduction systems allows a precise calculation of their frequency response. The calculation uses an electro-acoustic analog model for all elements constituting the system including the inlet ports, the pipes, the manifolds, and the sensor. The use of a dissipative transmission line model for pipes (Keefe, 1984) permits the introduction of viscothermal losses and time propagation in the calculation. An electro-acoustic analog schematic is generated for each noise-reduction system and the use of the matrix impedance of the schematic gives an easier computation of the pressure at each node of the circuit. The transfer function between each inlet and the output voltage of the sensor is calculated in the frequency domain. In the case of the rosette noise filters, the original principle presented in Alcoverro

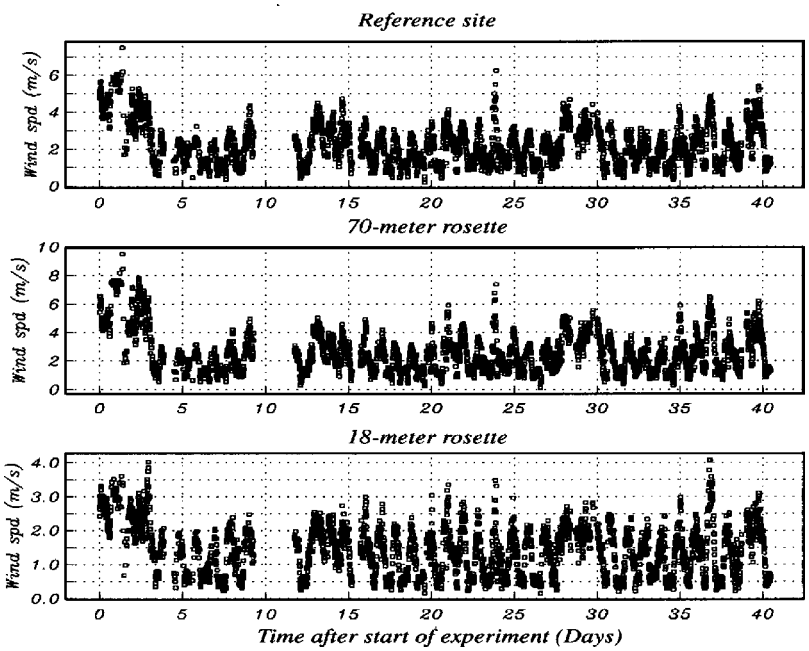

FIG. 6. Wind-speed data collected at the three sites. The panels from top to bottom represent data collected at the reference port, 70-m rosette filter and the 18-m rosette filter. Each symbol represents an average wind speed over a 15-min time interval. The experiment was interrupted briefly on day 10 by a telemetry fault. The experiment began during adverse weather conditions.

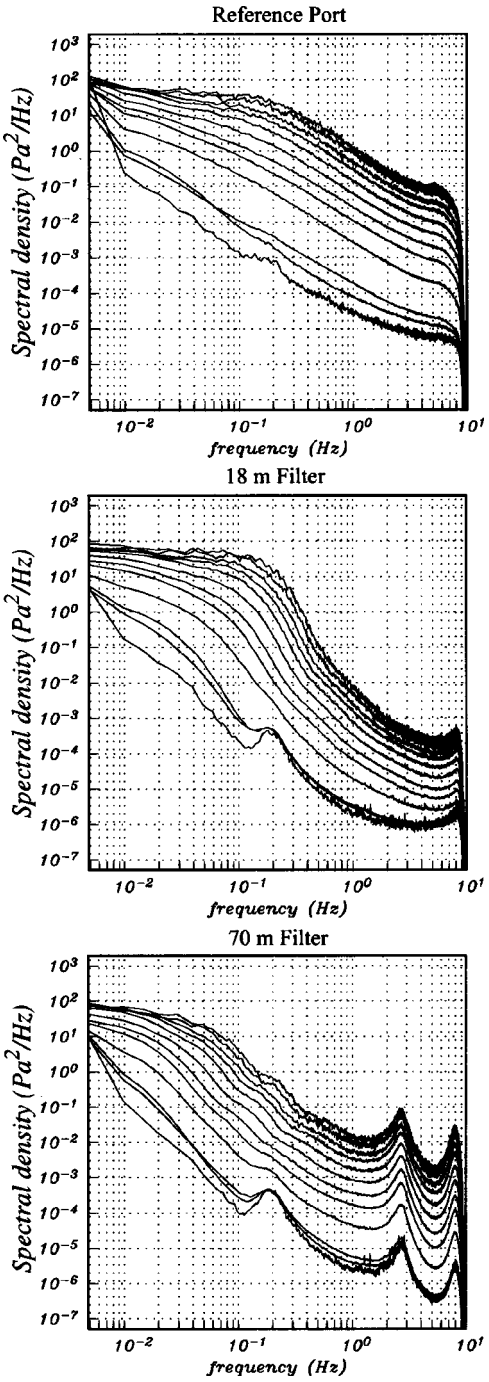

FIG. 7. The three panels in this figure show binned and stacked spectra taken at the reference port (top), 18-m rosette filter (middle) and 70-m rosette at wind speeds ranging from 0.0 to 0.5 m/s (lowest curve in each panel) up to 5.5 m/s in intervals of 0.5 m/s. The lowest curve in each panel represents spectral power at wind speeds below 0.5 m/s. The panels reveal a gradual increase in noise levels at all frequencies with wind speed at all sites. The microbarom peak is seen clearly near 0.2 Hz at all sites at wind speeds below 0.5 m/s, but is only seen in the filtered data at times when the wind speeds are above 0.5 m/s. Significant resonance peaks are seen above 1.0 Hz in the data from the 70-m filter.

(1998) gives an identical response for all inlets to ensure a perfect summation. In this case, the calculations are simplified and only one single-inlet transfer function needs to be calculated. The amplitude and phase response for 18-m/96-port and 70-m/144-port rosette filters is presented in Fig. 11. This simulation shows the frequency and amplitude for resonant peaks. In the case of a 70-m/144-port rosette filter, the first resonant peak is predicted at 2.69 Hz and the second at 8.08 Hz. It is essential that the sensor forevolume is considered in this calculation. A large forevolume acts like an active capacitance which would change the response of the overall system. The calculations presented in this paper used the known forevolume for the MB2000 sensor. The amplitude of the first resonance peak is estimated by comparing the measured noise spectra amplitudes between the this peak (at 2.65 Hz) and at 0.3 Hz. The amplitude difference, as seen in Fig. 12, is 17.9 dB. The same estimate, made from simulated noise spectra, gives an amplitude difference of 17.6 dB. The comparison between the measurements and the accurate electro acoustic calculation appears to validate the theory.

The bandpass amplitude of one inlet transfer function is equal to the inverse of the number of inlets. After summing a coherent wave passing over the noise reducer, the amplitude is equal to unity. These systems do not reduce the noise at frequencies lower than the first resonant peak. The frequency and amplitude of resonance, mainly induced by the length of the pipes, could be verified practically on the noise spectra measured with a real system.

The simulation of the noise reduction requires a wind model. The measurement of the coherence function between the noise generated by the wind at two points, separated by d meters, shows a linear increase of the coherence cutoff frequency as the wind speed increases, or the separation distance decreases. At low frequencies, the noise measured at the two points is coherent but not at high frequencies. The relation between the coherence cutoff frequency f_c, the mean wind speed v_m, and the separation distance d, is $f_c = 0.1 v_m / d$ (Alcoverro, 1998). A separate realization of random noise high-pass filtered above f_c is created for each inlet. The cutoff frequency is f_c, to respect the coherence criteria between these inlet and the others, at a given mean wind speed (Alcoverro, 1998). The synthetic noise generated for each inlet is convolved with the delayed impulse response of each transfer function (calculated in the frequency domain). The delays are determined by the geometric position of the inlet and the main wind direction. The global response of the system to a wind-speed condition is calculated by summing all convolutions. As the synthetic noise is not representative of the amplitude of noise, the results must be presented as the difference between the spectra of the noise applied at one inlet (noise generated by the wind at one point) and the spectra of the global response. The simulated noise reduction of the 70-m/144-rosette filter is presented in Fig. 12 for various mean wind speeds between 0.75 and 5.25 m/s.

Predicted noise reduction as a function of wind speed compares favorably with observed levels. The observed values are shown in the lower panel of Fig. 12. At all wind speeds, except those at or below 1.25 m/s, the theory accurately predicts the amount of noise reduction. The corner frequency of the noise reduction increases with increasing wind speed as predicted by theory. The location and width of the resonance peak is predicted accurately by theory. The location of the peak is determined by phase shifts and by the delay time between successive reflections inside the pipes.

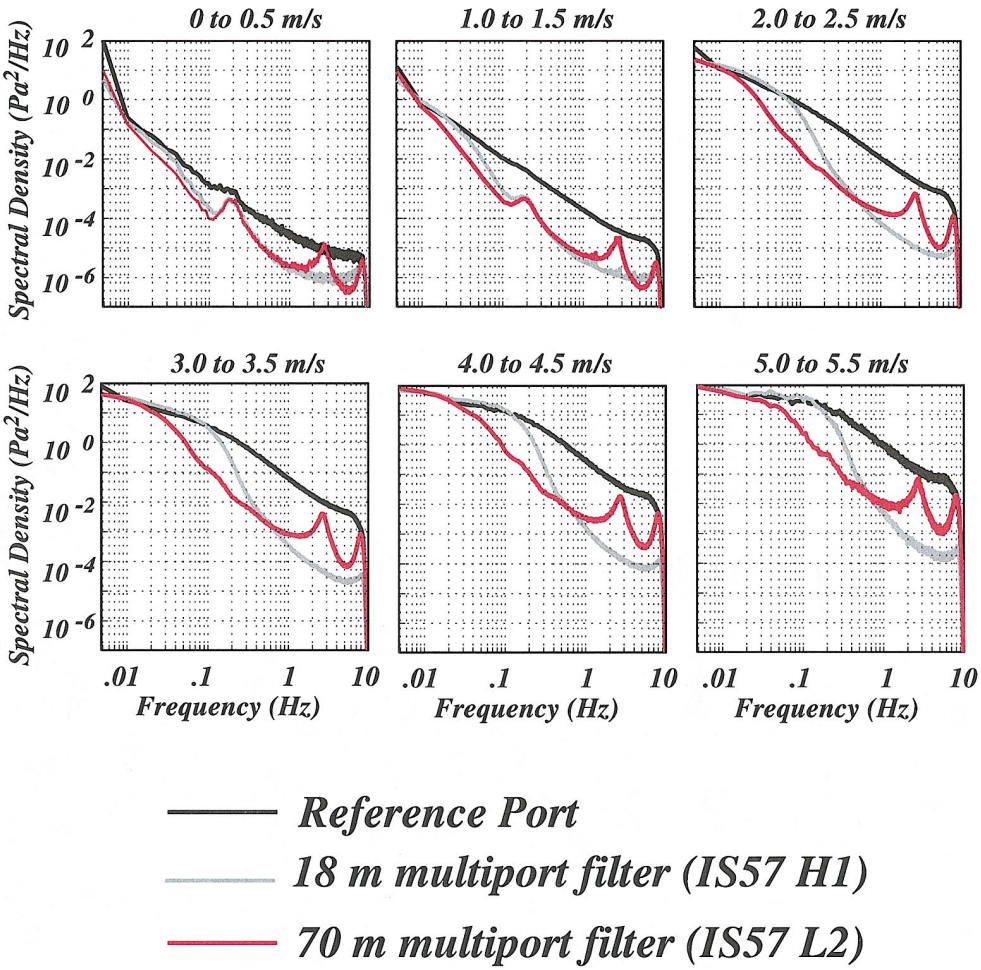

FIG. 8. A direct comparison of stacked spectra from the three different systems shows the growth of infrasonic noise levels at all sites with increasing wind speed. The increase in noise power with increasing wind speed is most significant at frequencies above 0.1 Hz. The 70-m rosette filter provides the most significant noise reduction at frequencies below 0.5 Hz. Large peaks above 1.0 Hz are seen only in the data from the 70-m filter. These peaks are not from the natural environment but are an artifact of the large filter.

The significant difference between observed and predicted noise levels near the microbarom peak at low wind speeds (1.25 m/s or less) stems from a higher level of coherence in the noise than is allowed for in the noise model.

VII. CALIBRATION OF ROSETTE FILTERS USING ACOUSTIC SIGNALS

A. Plane-wave response

Ambient noise, that has little or no coherence between inlets, can be used to study the effect of internal resonance on recorded data. Incoherent noise cannot, however, be used to calibrate the response of the filter to incoming plane waves. This response depends on time delays between the inlets in addition to resonance of the energy once it enters the pipe system. The rosette array is designed for vertically incident energy. Neglecting the resonance and dispersion inside the narrow pipes (Benade, 1968) that connect the inlets to the microbarometer, the filter should cause minimal distortion of signals arriving from directly above. The time delays between inlets become significant as the phase velocity of the signal decreases and approaches the ambient sound speed (i.e., when the signal arrives at grazing angles above the horizontal). For example, a signal that arrives with a phase velocity of 347 m/s (the sound speed at an air temperature of 27 °C) crosses an 18-m rosette filter in 0.05 s and a 70-m rosette filter in 0.2 s. Although the maximum phase delay for such energy recorded by an 18-m rosette is a quarter of the period of 5-Hz energy, this time delay is significant if the energy is recorded by a 70-m rosette.

Some atmospheric phenomena are known to produce signals with very high phase velocities. One notable example is aurora, which are known to produce acoustic waves at

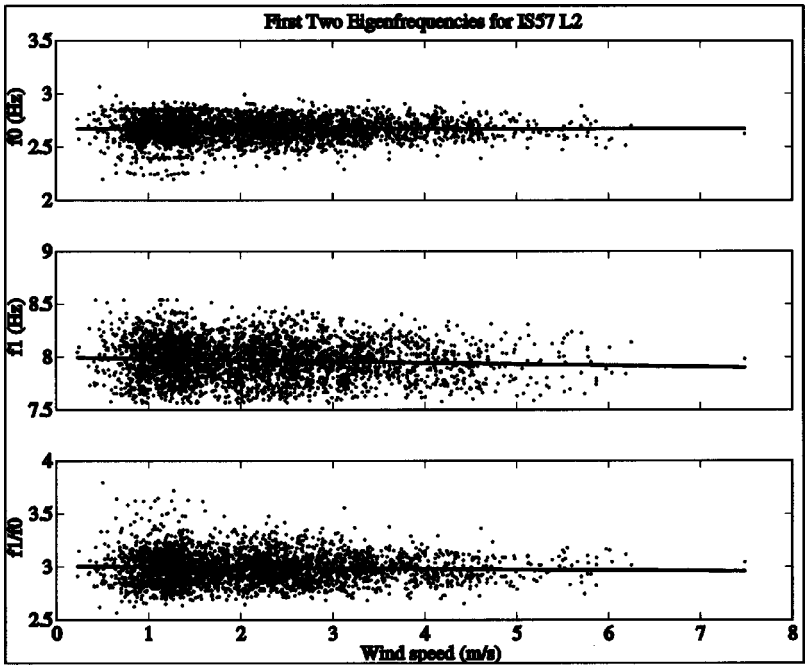

FIG. 9. Figures 7 and 8 reveal two significant peaks above 1.0 Hz in the spectra taken from the 70-m rosette filter. The center frequency of the two peaks in each of the 3074 spectral estimates is plotted in the upper two panels as a function of wind speed. The ratio of the two frequencies is given in the lower panel. The scatter observed in all panels is due to the inherent instability of the individual, unstacked, spectral estimates. We observe essentially no dependence of the peaks on wind speed. The ratio of the two frequencies is almost exactly 3.0.

phase velocities between 400 and 1200 m/s (McKisic, 1997). From ray theory, the phase velocity of an arrival equals the phase velocity at its turning point. As a result, high-phase velocity arrivals turn in the thermosphere; however, such arrivals are highly attenuated. Signals from most manmade sources and natural atmospheric phenomena in the lower atmosphere turn in the stratosphere and propagate across Earth's surface at phase velocities below 360 m/s (McKisic, 1997). At an air temperature of 27 °C, a phase velocity of 360 m/s is consistent with an arrival angle of 15° from the horizontal.

The plane-wave response of 18- and 70-m rosette filters is given in Fig. 13. As the figure shows, the 70-m filter response has a strong dependence on frequency for near-grazing angles of incidence. This frequency dependence is caused by destructive interference due to the relative time delays associated with propagation across the horizontal aperture of the space filters. At 5 Hz, the relative phase delays associated with the time delays of horizontal propagation

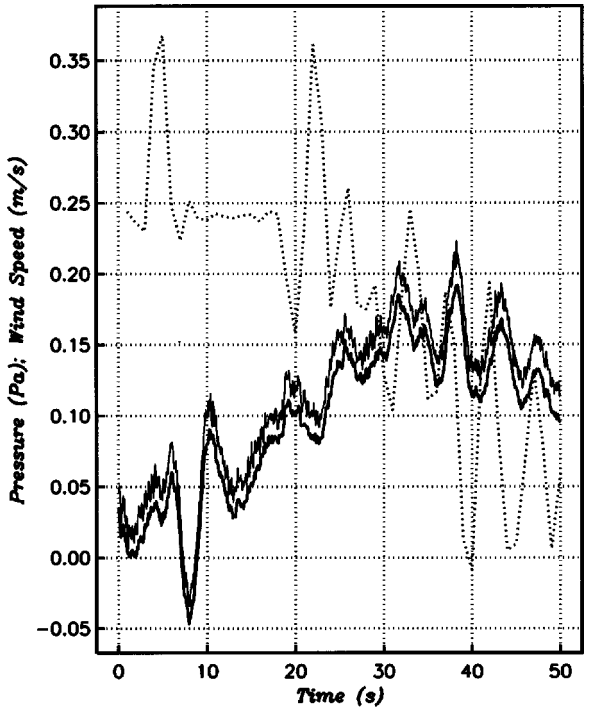

FIG. 10. The resonance occurring in the 70-m filter (upper solid curve) obscures much of the detail that is seen clearly in data from a colocated filter constructed of microporous hoses (lower solid curve beneath the black curve). The coarsely dashed curve shows the wind speed during the 50-s interval. This example shows that the resonance is significant even at times of essentially no wind.

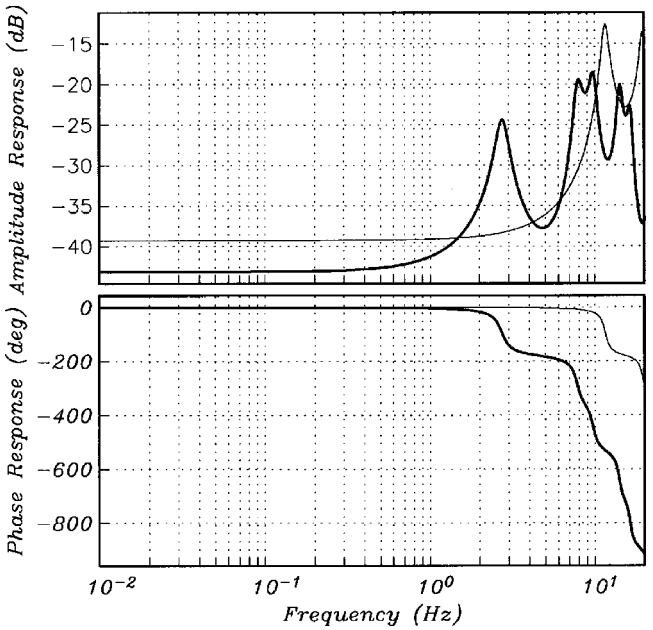

FIG. 11. Predicted amplitude and phase response of the 18-m/92-rosette filter (light curve) and the 70-m/144-rosette filter (bold curve) for one inlet. The resonance peaks coincide with significant change in the phase response of the filter. The long-period response is given by $-20\log_{10}(N)$, where N is the number of inlets.

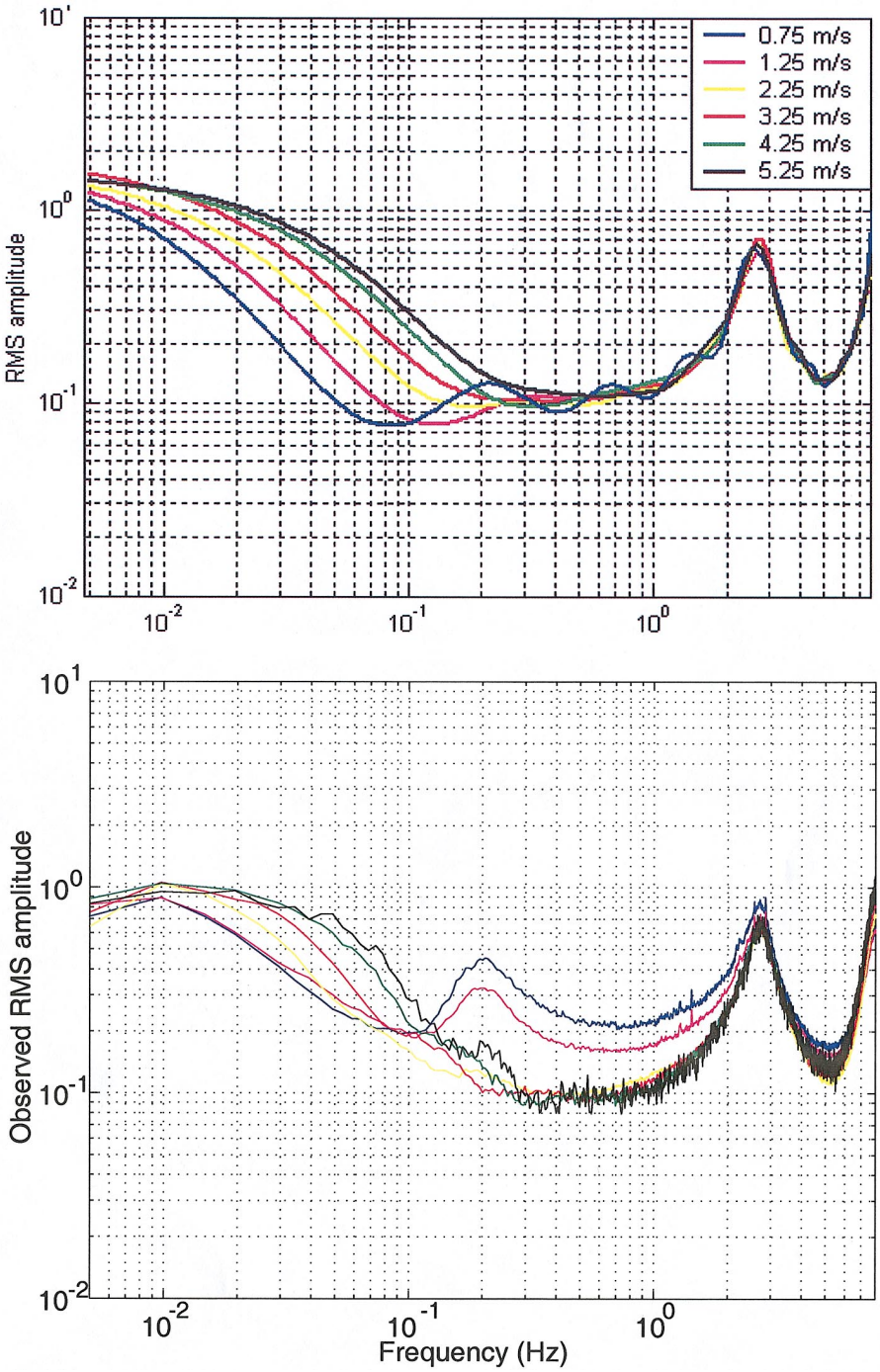

FIG. 12. Simulated noise reduction of the 70-m/144-port rosette filter for various mean wind speeds is shown in the upper panel. Each curve represents the ratio between the noise spectrum observed at the reference port and the noise spectrum of the rosette system. The corner frequency of the 70-m rosette filter is predicted to increase with increasing wind speed. Observed noise reduction is shown in the lower panel.

cause complete cancellation to occur. In effect, each space filter acts as an array of omnidirectional sensors where each port in the space filter represents a sensor. Since the propagation pathway from port to the summing manifold is identical for each port, the space filter array is mechanically beamformed so that its main lobe points in the broadside direction, i.e., in the vertical direction.

B. Analysis of a recorded signal

The theoretically derived amplitude and phase response of rosette filters that takes into account both the time delays between inlets and resonance of the energy once it has entered the pipe system can be tested by analyzing signals recorded via the filters. The ideal signal for this purpose has a long duration, a large amplitude, and arrives at a time of low ambient noise levels so there will be minimal interference with the noise the filter is designed to remove. This signal has a low phase velocity so that time delays between inlets in the filter will be large. As shown by Fig. 13, a signal arriving with a high phase velocity would only allow us to test further the theory of resonance inside the pipes as time delays between the inlets would be negligible. The ideal signal is generated by a well-documented source. Finally, to allow extraction of the amplitude and phase of a rosette filter, it is also necessary to record the ideal signal not only with the rosette filters, but by a microbarometer that is not attached to a noise reduction system, but is attached to a single inlet located at the center of the rosette filter.

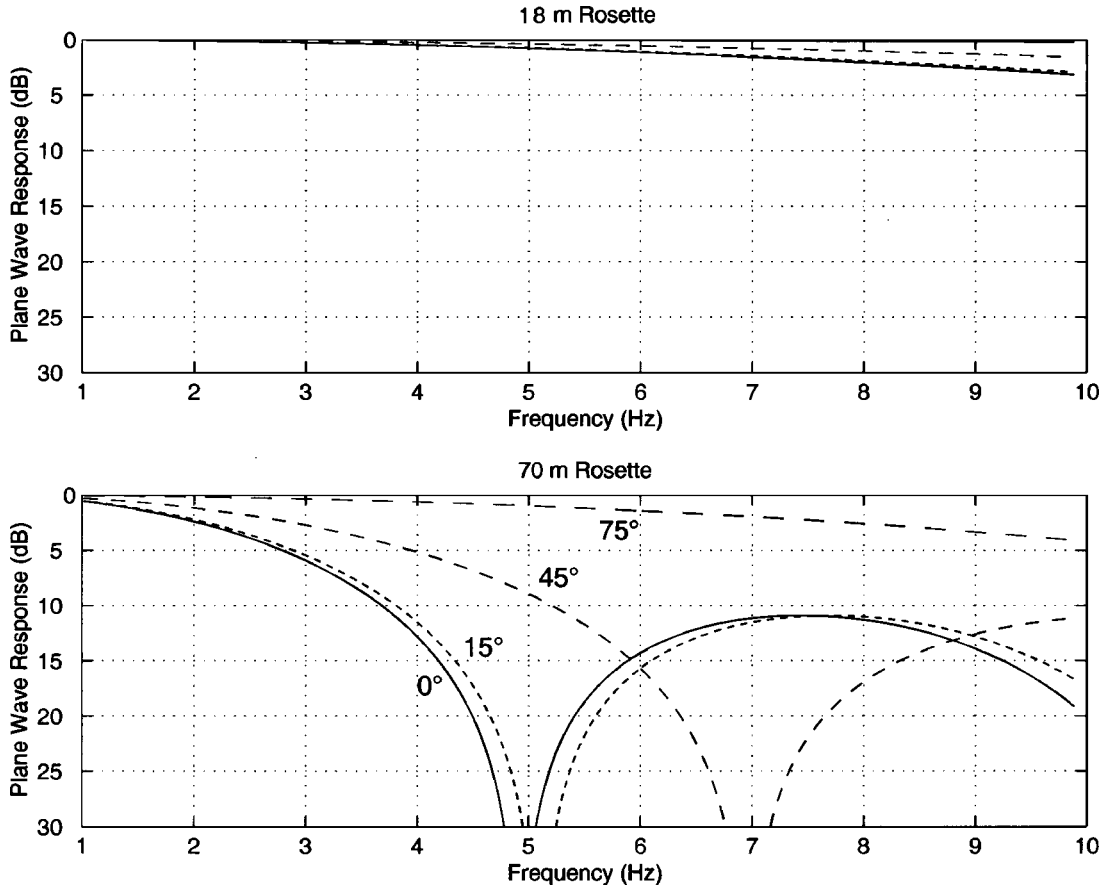

FIG. 13. In the upper and lower panels we show the plane-wave response for the 18- and 70-m rosette filters, respectively, at four arrival angles. The solid curves in each panel represent the response to horizontally propagating signals. The finely to coarsely dashed curves represent signals propagating across the two filters at 15°, 45°, and 75° above the horizontal. The elevation angles, θ_e, are calculated assuming a sound speed, c, of 347 m/s. The phase velocity, c_p, is given by $c/\cos(\theta_e)$. The phase velocities corresponding to the arrival angles at the four arrival angles are 347, 359, 491, and 1341 m/s.

Such a signal occurred on 23 April 2001. On that day, a meteor exploded off the west coast of North America with a yield of several kilotons (Garces *et al.*, 2001). Satellite data places the location of the explosion at 28.6 °N, 134.2 °W at an altitude of 30 km (Brown and Gault, 2001). This location is approximately 1800 km to the west of the Pinon Flat Observatory. This event was recorded by infrasound arrays across North America and as far away as Germany (Garces *et al.*, 2001). The explosion was recorded by the Pinon IMS array I57US and by all sites in our noise experiment. The experiment included the 18- and 70-m rosette filters that are the subject of this paper. The experiment also included noise collected by MB2000 microbarometers via single reference ports located at the center of each rosette filter. The explosion occurred at 06:09 UT and thus the signals arrived at the Pinon flat observatory near midnight local time (Fig. 14).

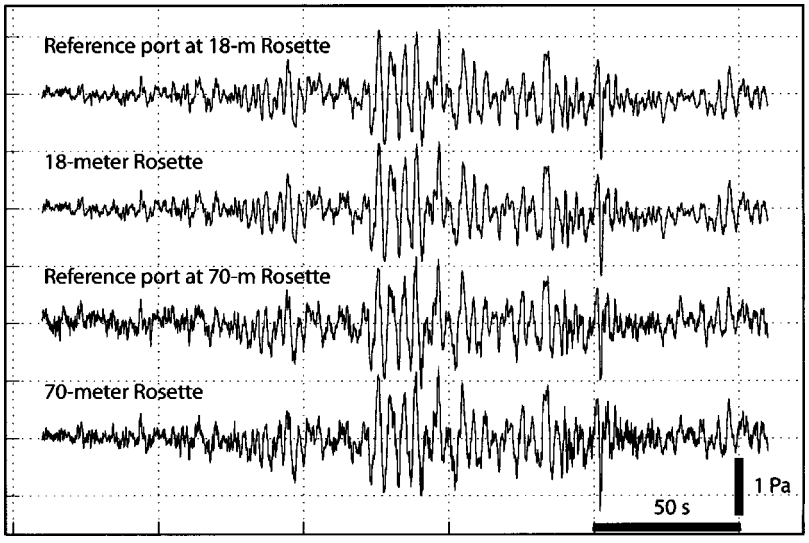

FIG. 14. The widely reported explosion of a large meteor off the coast of California on 23 April 2001 was recorded by the IMS array 157US at PFO and by sensors in our wind-noise experiment. We show recordings made by 18- and 70-m rosette filters at sites H1 and L2, respectively, in the infrasound array 157US via reference ports at the same locations. The H1 and L2 sites are ~600 m apart (Fig. 3). The recordings reveal the signal to be highly coherent. The maximum amplitude of the signal was ~2 Pa peak-to-peak. The duration of the coherent energy was ~200 s. The recordings shown in this figure are unfiltered.

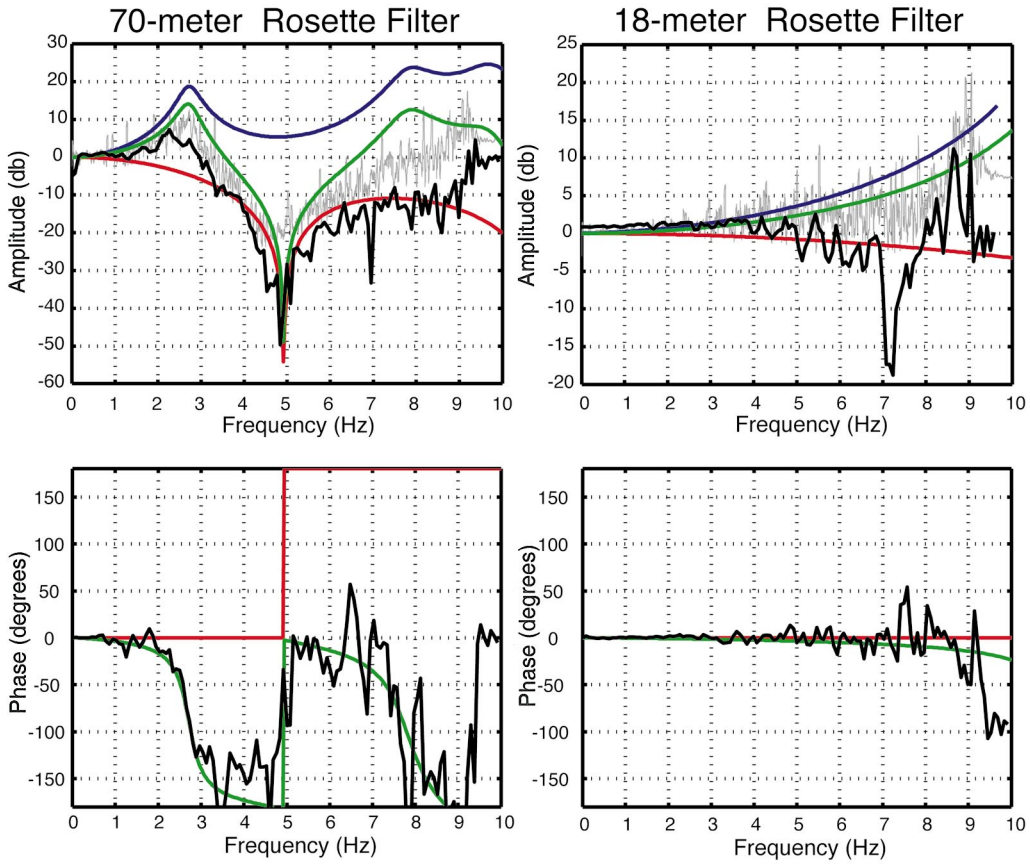

FIG. 15. Amplitude and phase response of 18- and 70-m rosette filters are shown in this figure. The blue curves in all panels represent the response due to internal resonance inside the pipe systems. The red curves represent the plane-wave response. The plane-wave response was calculated assuming a phase velocity of 330 m/s. This is the phase velocity of the energy from the 23 April bolide as determined by processing data from the 157US array. The green curves represent the total response due to time delays between inlets and to resonance inside the filters. Amplitude and phase from a phase-coherent cross-spectral analysis of data from the 23 April bolide are shown in black. The theory accurately predicts the phase of the signal but underpredicts the amplitude at all frequencies. A spectral ratio of the filtered to unfiltered data (gray curves in the upper panels) closely matches the theoretical predictions. The green curves in the lower panels plot on top of the blue curves except in the lower left panel above 5 Hz. At those frequencies the phase of the internal resonance in the 70-meter filter is less than −180 (Fig. 11).

Due to the strong diurnal cycle in infrasonic noise levels, local noise levels at that time were minimal. The wave train of arrivals remained above noise for >200 s and reached a maximum amplitude of 2 Pa peak-to-peak. Brown and Gault (2001) observed the signal was highly coherent across the Pinon array. The signal propagated across the array with a very low phase velocity of 330 m/s (D'Spain *et al.*, 2001). This corresponds to an arrival angle close to 0° above the horizontal. Signal is observed clearly above noise across the broad band from 0.05 to 7.0 Hz. This signal provides an opportunity to gauge the utility of the various noise reducing devices at preserving coherent signals from remote sources while reducing noise.

Two signal-processing approaches based on linear time-invariant filter theory can be used. In a phase-coherent approach, both the amplitude and phase response of a filter as a function of frequency are estimated by normalizing the cross spectrum Sxy between the input and output time series by the autospectrum of the input Sxx (Bendat and Piersol, 1986)

$$H(f) = Sxy(f)/Sxx(f). \tag{1}$$

The microbarometer located in the center of the space filter but not connected to any mechanical filtering system provides the input time series $[x(t)]$ and the signal recorded by the microbarometer connected to the space filter provides the output time series $[y(t)]$. The results of using this approach with nearly 1 min, 45 s of time series containing the majority of the arriving energy from the bolide are plotted as a black curve in Fig. 15. For the phase responses (lower two panels), the agreement between the data from the bolide and the theory (plotted as green curves) is excellent, particularly for the 70-m space filter. In the case of the amplitude responses, the overall spectral shape of the measured and predicted responses are in general agreement. However, the measured amplitude response is lower than predicted and appears to diverge with increasing frequency. This difference suggests that a frequency-dependent attenuation mechanism is not being accounted for in the theory.

A second approach is phase incoherent and so only provides information on the amplitude of the filter response. It is obtained simply by taking the square root of the ratio of the output autospectrum to the input autospectrum (Bendat and Piersol, 1986)

$$|H(f)| = (Syy(f)/Sxx(f))^{0.5}. \tag{2}$$

The results of this technique using exactly the same segment

of data as in the phase-coherent calculation are shown as gray curves in the upper panels of Fig. 15. They are generally in better agreement with theory. These transfer-function amplitude estimates from Eq. (2) are larger because of the addition of a component in the time series of the microbarometer with space filter that is phase uncorrelated with the reference microbarometer time series.

VIII. CONCLUDING REMARKS

To monitor Earth's atmosphere for weak signals from small nuclear tests anywhere on the globe requires that we develop an effective means to filter out noise due to atmospheric turbulence. For the International Monitoring System network under current development, rosette spatial filters are the first choice for new sites. In this study, we have examined the utility of these filters for removing incoherent noise across a broad band while preserving coherent signals.

A. Noise reduction

With minor exceptions, our observations of noise reduction provided by the 18- and 70-m filters are predicted by the theoretical method of Alcoverro (1998). The theory underpredicts coherence near the microbarom peak as this energy is propagated acoustically, not by turbulent wind. In some cases noise reduction provided by the 18-m filter exceeded the limit predicted assuming perfectly incoherent noise. This anomaly does not reflect an error with the theory but is due to the 18-m filter receiving some shelter from prevailing winds by nearby vegetation.

Data from our experiment, and from analytical simulations, attest to the utility of these filters for reducing noise at frequencies of interest to the nuclear monitoring community. We have observed, however, that the performance of the filters is severely degraded at all wind speeds by resonance. The most significant resonance occurs within the long pipes that connect the secondary summing manifolds with the microbarometer, or the primary summing manifold at the center of the filter. The resonance in the 18-m filter is observed above 3.0 Hz and is less important as nuclear monitoring relies mainly on lower frequencies. Resonance in the 70-m filters is significant at frequencies above 0.7 Hz.

Experiments indicate that the low-frequency resonance can be removed by placing impedance-matching capillaries in the long pipes connecting the summing manifolds (Hedlin, 2001). The results of this work will be reported in detail in a future paper.

Temperature changes at the recording site will cause sound-speed-sensitive changes in filter response characteristics. However, these changes are found to be insignificant if the pipes are buried and thus protected from large temperature swings.

B. Frequency-dependent directionality of the space filters

Rosette filters are designed for maximum effectiveness for vertically arriving signals. The directionality is not significant for low-frequency signals regardless of the arrival direction. Signals above 1 Hz arriving at grazing angles ($<15°$ from the horizontal) are severely attenuated by the 70-m rosette filters.

A cross-spectral analysis of signals from the explosion of bolide over the Pacific provided an opportunity to further test the resonance theory, to validate an extended theory that takes into account both the resonance and the plane-wave response of the rosette filters, and to calibrate the filters. The combined theory accurately predicts the phase response of the filters; however, the measured amplitude response is lower than predicted, suggesting that attenuation is not fully accounted for in the theory. The good agreement of predicted and observed phase shifts, as well as the general agreement with the phase-incoherent derived amplitudes with those derived from the theory, indicate that the theoretical method is sound and can be used to predict the response of the filter to signals that propagate across the filters at other velocities.

ACKNOWLEDGMENTS

The authors are indebted to Doug Christie (CTBTO) for ongoing assistance with this project. Frank Vernon, Jennifer Eakins, and Glen Offield provided the real-time data link. Clint Coon provided field assistance. The authors would like to thank Lou Sutherland and Milton Garces for many helpful comments on this paper. Funding was provided by the Defense Threat Reduction Agency under Contract No. DTRA01-00-C-0085. Funding for the rosette filters used in this study was provided by the Defense Threat Reduction Agency, the Provisional Technical Secretariat (PTS) of the UN Comprehensive Test Ban Treaty Office in Vienna, and the US Army Space and Missile Defense Command (SMDC) University Research Initiative (URI).

Alcoverro, B. (**1998**). ''Proposition d'un systeme de filtrage acoustique pour une station infrason IMS,'' CEA-DASE Scientific Report, No. 241.

Benade, A. H. (**1968**). ''On the propagation of sound waves in a cylindrical conduit,'' J. Acoust. Soc. Am. **44**, 616–623.

Bendat, J. S., and Piersol, A. G. (**1986**). *Random Data Analysis and Measurement Procedures* (Wiley, New York).

Blanc, E. (**1985**). ''Observations in the upper atmosphere of infrasonic waves from natural or artificial sources: A summary,'' Ann. Geophys. (France) **3**, 673–688.

Broche, P. (**1977**). ''Propagation des ondes acoustico-gravitationnelles excitees par des explosions,'' Ann. Geophys. (C.N.R.S.) **33**, 3, 281–288.

Brown, D. J., and Gault, A. K. (**2001**). ''Observations and Preliminary analysis of the northern Pacific infrasonic event,'' 23 April, 2001, Center for Monitoring Research technical report CMR-01/09, 21 May, 2001.

Burridge, R. (**1971**). ''The acoustics of pipe arrays'' Geophys. J. R. astr. Soc. **26**, 53–69.

Calais, E., Minster, J. B., Hofton, M. A., and Hedlin, M. A. H. (**1998**). ''Ionospheric signature of surface mine blasts from Global Positioning System measurements,'' Geophys. J. Int. **132**, 191–202.

D'Spain, G., Hedlin, M. A. H., Orcutt, J. A., Kuperman, B., DeGroot-Hedlin, C. D., Berger, L., Rovner, G., and Hudak, H. (**2001**). ''Bolide, Rocket Launch, and Background Infrasonic Noise Recordings at I57US and Anza Temporary Stations,'' Infrasound Technology Workshop, 12–15 November 2001, Kailua-Kona, Hawaii.

Daniels, F. B. (**1950**). ''On the propagation of sound waves in a cylindrical conduit,'' J. Acoust. Soc. Am. **22**, 563–564.

Daniels, F. B. (**1959**). ''Noise reducing line microphone for frequencies below 1 c/s,'' J. Acoust. Soc. Am. **31**, 529.

Davidson, M., and Whitaker, R. W. (**1992**). ''Miser's Gold,'' Los Alamos National Laboratory Technical Report: LA-12074-MS.

Francis, S. H. (**1973**). ''Acoustic-gravity modes and large-scale traveling ionospheric disturbances of a realistic, dissipative atmosphere,'' J. Geophys. Res. **78**, 13, 2278–2301.

Garces, M., Hetzer, C., Lindquist, K., Hansen, R., Drob, D., and Picone, M. (**2001**). ''Stratospheric arrivals in the upstream wind direction: Case study of the 23 April, 2001 bolide,'' Infrasound Technology Workshop, 12–15 November, 2001, Kailua-Kona, Hawaii.

Grover, F. H. (**1971**). ''Experimental noise reducers for an active microbarograph array'' Geophys. J. R. Soc., **26**, 41–52.

Hedlin, M. A. H. (**2001**). ''Recent experiments in infrasonic noise reduction: The search for that elusive broadband filter,'' Infrasound Technology Workshop, 12–15 November 2001, Kailua-Kona, Hawaii.

Hedlin, M. A. H., Berger, J., and Vernon, F. (**2002**). ''Surveying infrasonic noise on oceanic islands,'' Pure Appl. Geophys. **159**, 1127–1152.

Herrin, G., Golden, P., and Hedlin, M. A. H. (**2001**). ''Investigation of wind noise reducing filters,'' Infrasound Technology Workshop, 12–15 November 2001, Kailua-Kona, Hawaii.

Kaimal, J. C., and Finnigan, J. J. (**1994**). *Atmospheric Boundary Layer Flows: Their Structure and Measurement* (Oxford University Press, Oxford).

Keefe, D. H. (**1984**). ''Acoustical wave propagation in cylindrical ducts; Transmission line parameter approximations for isothermal and nonisothermal boundary conditions,'' J. Acoust. Soc. Am. **75**(1), 58–62.

Lamb, H. (**1932**). *Hydrodynamics*, 6th ed. (London).

Landau, L. D., and Lifshitz, E. M. (**1959**). *Fluid Mechanics* (Pergamon, Oxford).

McKisic, J. M. (**1997**). ''Infrasound and the infrasonic monitoring of atmospheric nuclear explosions: A literature review,'' Final report submitted to the DOE and Phillips Lab, PL-TR-97-2123.

Priestley, J. T. (**1966**). ''Correlation studies of pressure fluctuations on the ground beneath a turbulent boundary layer,'' Washington D.C., National Bureau of Standards Report No. 8942, U.S. Dept. of Commerce, National Bureau of Standards.

Sereno, T. J., and Orcutt, J. A. (**1985**). ''Synthesis of realistic oceanic Pn wave trains,'' J. Geophys. Res. **90**, 12755–12776.

Simons, D. J. (**1995**). ''Atmospheric methods for nuclear test monitoring. Monitoring a comprehensive test ban treaty,'' NATO ASI series E, Vol. 303, pp. 135–141, edited by E. S. Husebye and A. M. Dainty.

Welch, P. D. (**1967**). ''The use of fast Fourier transform for the estimation of power spectra: A method based on time averaging over short, modified periodograms,'' IEEE Trans. Audio Electroacoust. **AU-15**, 70–73.

Zumberge, M. A., Berger, J., Hedlin, M. A. H., Husmann, E., Nooner, S., Hilt, R., and Widmer-Schnidrig, R. (**2003**). ''An optical fiber infrasound sensor: A new lower limit on atmospheric noise between 1 and 10 Hz,'' J. Acoust. Soc. Am. **113**(5), 2474–2479.